Indian Journal of Pure & Applied Physics
Vol. 62, October 2024, pp. 864-874
DOI: 10.56042/ijpap.v62i10.12586

Augmentation of Isolation and Bandwidth of Compact MIMO Antenna for UWB Applications

Mohd Azharuddin, Kalyan Mondal* & Deepak Kumar Barik
Department of Electronics and Communication Engineering, National Institute of Technology Manipur, Imphal 795 004, India

Received 18 July 2024; accepted 9 September 2024

A Multiple Inputs Multiple Outputs (MIMO) antenna with a compact dimension of $0.28\lambda_0 \times 0.36\lambda_0$ for ultra-wideband (UWB) spectrum applications has been proposed, where, λ_0 is the free space wavelength at the resonating frequency of 3.34 GHz. The proposed work consists of two identical radiating antenna elements and a modified T-shaped ground structure with a loaded rectangular slot. The modified T-shaped structure greatly affects impedance matching and electromagnetic field distribution. Due to that, the impedance bandwidth, isolation, compactness, and other MIMO parameters are also enhanced. The proposed antenna confirms a measured UWB frequency of 3.0 - 11.66 GHz. The antenna isolation greater than 20 dB throughout the working spectrum is achieved. The results further signify that the antenna displays good MIMO performance with respect to envelope correlation coefficients (ECC), diversity gain (DG), channel capacity loss (CCL), and gain. The ECC value of less than 0.01, diversity gain above 9.98 dBi, peak gain of 3.52 dBi, and CCL lesser than 0.25 bits/S/Hz are achieved. The group delay and phase response are also studied for ensuring distortion-less signal transmission under broad impedance bandwidth.

Keywords: MIMO; Ultra-wideband (UWB); Isolation; Gain; ECC; DG; CCL

1 Introduction

In present-day wireless communication systems, there is an utmost need of higher data rate, power efficiency, low-priced with high security[1]. In 2002, the FCC (Federal Communication Commission) had allotted the frequency spectrum from 3.1 GHz to 10.6 GHz for ultra-wideband (UWB). Research on ultra wideband technology has been widely conducted since then and also because of its advantage over narrowband systems and wide area of applications. The narrowband systems experience low data throughput and low reliability. Moreover, UWB systems experience multipath fading which results in low data carrying capacity, low reliability and very sensitive to locations of transmitting and receiving antennas. This effect is minimized by implementing Multiple Inputs Multiple Outputs (MIMO) antenna systems[2-3]. Therefore, UWB technology is incorporated with MIMO technology to achieve high data throughput, high channel capacity and better link quality. So, without disturbing the available spectrum or the power consumption rate, wireless portable devices and base stations are equipped with diversity techniques[4]. Hence, number of UWB antennas is provided to support this technology[5-9]. High speed mobile communications, emergency services, RADAR, tracking with high spatial resolution, roadside assistance and in-car sensor network communication are some of the applications in which UWB MIMO technology is incorporated with[10]. In MIMO communication systems, numerous data streams are transmitted by the transmitter with multiple antennas and are received by the receiver with multiple antennas. At the same time, the antenna elements belonging to the transmitter and the receiver should be provided with high isolation. However, deployment of multiple antennas in a limited space leads to severe mutual coupling. Thus, numerous methods have been offered to improve the isolation which includes engraving a slot out of the ground. In[11], the ground has been introduced with circular ring so that the wideband (WB) MIMO antenna is decoupled throughout the operating band. In[12], isolation of more than 20dB is achieved between the antenna elements with the incorporation of Isolating metallic sheet (IMS). Greater isolation is obtained by introducing defected ground structure and parasitic elements[13-14]. In[15], UWB MIMO antenna uses a strip reflector made of metal to acquire greater isolation of 20dB. In[16], isolation greater than 22dB is achieved by employing neutralization line

*Corresponding author: (E-mail: kalyankgec@gmail.com)

between the monopoles. In[17], bi-planar Yagi-like UWB MIMO antenna is proposed with isolation higher than 17 dB. In[18], isolation of 25dB is obtained by employing a fench-type decoupling structure with 8 GHz bandwidth. Moreover, higher isolation is obtained by putting the antennas perpendicular to each other in[19-22]. In[23], high isolation is obtained by employing parasitic stubs between antenna elements. Offset feed, Inkjet-Printed, Fench-type and Inverted-A based compact decoupling structure are also being used to improve the isolation[24-26]. In[27], an electromagnetic band gap (EBG) structure is made to use to improve the isolation between square shaped radiators. Metamaterials are used to diminish the size of antenna and reduce mutual coupling[28]. In[29], isolation is increased by the ground plane truncation with rectangular slots via ellipsoid slot. In[30], enhancing the isolation is accomplished by engaging decoupling and common defected ground approach, thus improving the isolation to more than 28dB. Moreover, other approaches such as using a Machine Learning (ML) approach to optimize antenna parameters to the desired level are found in[31-33].

This paper proposes and analyzes an UWB MIMO antenna, having a compact dimension of $25 \times 32 \times 1.6mm$. The antenna possesses two identical antenna elements. A modified T-structure is utilized as a ground stub to improve impedance bandwidth along with the isolation. The ground is incorporated with an additional rectangular slot to further expand the bandwidth along with providing better isolation. Results of simulation and measurement confirm that there is a minimum discrepancy between the two results. Moreover, ECC, DG, CCL, Gain, group delay and phase response confirm the decent performance of the proposed UWB MIMO antenna.

2 Antenna Design Process and Working Mechanism

This section discusses the design procedure and analysis of the UWB MIMO antenna, shown in Fig. 1. Then it is followed by the evolution steps starting from Ant.0 to Ant. IV (prop.). The evolution steps are associated with the usage of various ground stubs and slots to be able to accomplish the proposed UWB MIMO. Further, the impact of ground stubs and slots are discussed. Then the impact of various ground stubs and slot is described subsequently where S-parameter, surface current distributions with either port excited and other terminated, Gains, maxima and minima isolation, efficiency etc. are also elaborated. Furthermore, radiation mechanism of the monopole antenna element is also discussed. Lastly, parametric studies are carried out to verify the final parametric dimensions and the corresponding simulated and measured results.

2.1 Design Procedure of UWB MIMO Antenna

The design of the antenna is carried out in stepwise manner. The various steps leading to the final and proposed MIMO antenna are shown in Figs. 1 (a)-(e).

The antenna is fabricated on FR4 substrate having dielectric constant of ε_r=4.4 with loss tangent of tan δ=0.02. The antenna occupies a compact size of $25\times32\times1.6mm^3$. It possesses two similar antenna elements (monopole) Antenna 1 and Antenna 2 with identical dimensions on the top side of the substrate. The configuration of the MIMO antenna is presented in Fig. 2(a).

There are different shapes of antenna elements such as elliptical, rectangular, ring or circular[34-36]. However, the main challenges the UWB antenna designers are facing are to reduce the size of antenna elements so that the overall antenna system could be

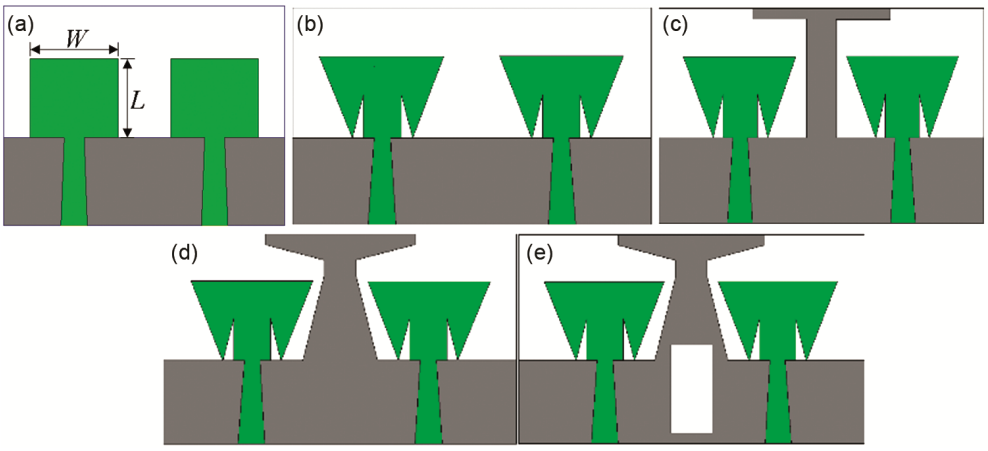

Fig. 1 — Antenna design steps (a) Ant.0 (b) Ant. I (c) Ant. II (d) Ant. III and (e) Ant. IV (prop)

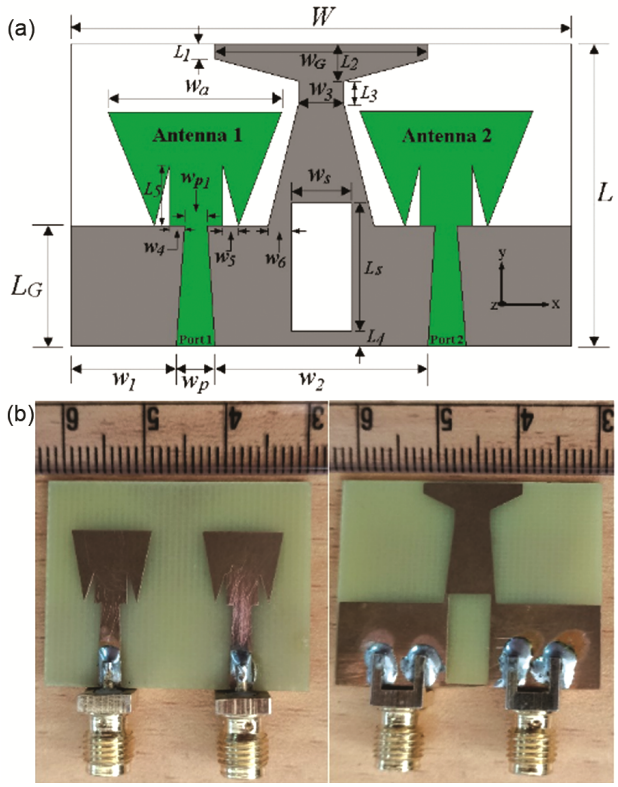

Fig. 2 — Antenna design structure of (a) Proposed MIMO and (b) Fabricated MIMO

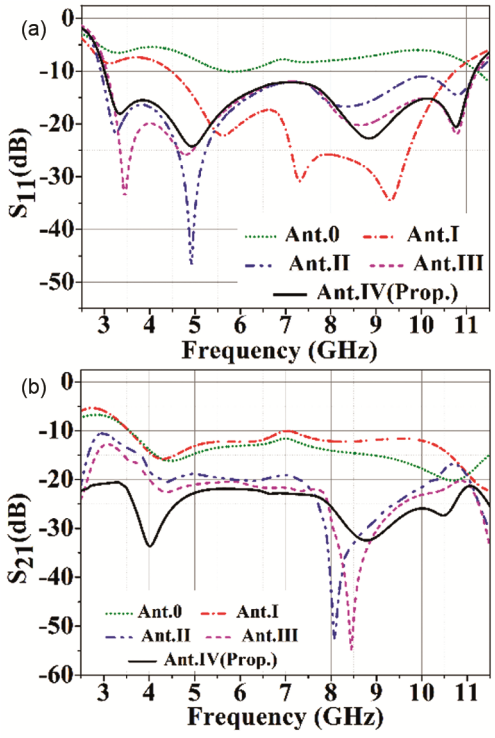

Fig. 3 — S-Parameter characteristics of Ant.0 to Ant.IV (a) $|S_{11}|$ (b) $|S_{21}|$

made more compact. This can be achieved when low resonance is generated which is possible when the size of the antenna elements is such that it provides a long current path. Thus, a cut-off frequency lower than 3.1 GHz can be achieved to meet the UWB frequency requirements. Moreover, the antenna elements are fed by a tapering feed line. This prevents the creation of a notched frequency spectrum ranging from 6.54 GHz to 7.48 GHz.

To enhance the impedance matching, a T-structured ground stub is utilized as shown in Fig. 1(c) as ground stub between the antenna elements which increases the bandwidth but the isolation is still lower than 15dB at lower frequency regions. To further improve the isolation, the T-structure is modified as shown in Fig. 1(d). Moreover, vertical rectangular slot is carved out of the ground to produce the proposed and final MIMO antenna as shown in Fig. 1(e). As a result, the isolation is more enhanced to more than 20dB throughout the working spectrum. This can be confirmed from the resulting S-parameter graph shown in Fig 3. The antenna elements have got similar structure so that input ports must have equal impedances. The antenna design is accomplished by using HFSS 13.0 on FR4 substrate. The final enhanced parameters for the antenna are given in Table 1. These parameters are utilized to manufacture the antenna model presented in Fig. 2(b) (Fabricated antenna) for the measurement purpose.

2.2 Working Mechanism

2.2.1MIMO antenna radiation technique

We are already aware that the proposed UWB MIMO antenna possesses two quarter- wavelength ($\frac{\lambda_g}{4}$) monopole antennas as shown in Fig. 1(a). For the effective radiation, the approximate length *L (=9mm)* of these monopole antennas is chosen and calculated by using Eq. 1-2[37].

$$L \approx \left(\frac{\lambda_g}{4}\right) = \frac{\lambda_0}{4\sqrt{\varepsilon_{eff}}} = \frac{c}{4f_0\sqrt{\varepsilon_{eff}}} \quad \ldots (1)$$

Where λ_0 is the free space wavelength at the lowest resonant frequency f_0.

Table 1 — Dimensions of the proposed MIMO antenna

Parameters	W_A	W_{p1}	W_a	W_p	W_1	W_2	--
Dimensions	32	2.26	10	3	6.5	13	--
Parameters	W_3	W_4	W_5	W_6	W_s	W_G	L_A
Dimensions	4.5	0.87	1.25	0.75	5	12.5	25
Parameters	L_G	L_S	L_1	L_2	L_3	L_4	L_5
Dimensions	10	10.5	1.5	3.5	1.5	0.5	4

$$\varepsilon_{eff} = \frac{\varepsilon_r + 1}{2} \quad \ldots (2)$$

Where ε_{eff} and ε_r are the approximate effective and relative permmitivity of the *FR4* substrate and *c* is the speed of light. The patch antenna is now excited with respect to ground. As fringing happens, the electromagnetic wave (EMW) radiates from the edge of the patch.

2.2.2 Isolation enhancement technique

To visualize the results of the use of the modified T-structure and the slot on isolation and bandwidth, the S-parameter and current distributions are used to further explore the evolution steps of the antenna from Ant.0 to Ant. IV (prop.) at 3.34 GHz which happens to be first resonance frequency. The corresponding S-parameter is shown in Fig. 3.

Fig. 3(a & b) show that Ant.0 and Ant. I display isolation below 15dB. The impedance bandwidth of Ant. I lies between 4.46 GHz and 10.72 GHz. Further, for Ant. II in which T-structure is used as ground stub, the impedance bandwidth and isolation are found to be improved compared to Ant. I. The impedance bandwidth lies between 2.92 GHz and 11.28 GHz while the isolation is more than15dB except at lower frequency regions. 15dB is the minimum acceptable isolation to be maintained[2] for optimum MIMO performance. However, with the T-structure being modified as in Ant.III, it is quite visible that the impedance bandwidth is found to be from 3.05 GHz to 11.22 GHz. The bandwidth is reduced as compared to that of Ant. II while the isolation is better in this case. However, the isolation is still lower than 15dB in the lower frequency region as shown in Fig. 3(b). Further, the effect of rectangular ground slot on isolation is observed in Ant. IV (prop.) in which impedance bandwidth is from 3.0 GHz to 11.22 GHz, wider than the impedance bandwidth provided by Ant. III while the isolation is found to be greater than 20 dB throughout the working spectrum. Thus, the rectangular slot aids in providing greater isolation and bandwidth from Ant. III to Ant. IV (prop.). Moreover, the surface current distributions are explored to confirm the effect of modified T-structure and the slot for the evolution steps of the antenna from Ant. I to Ant. IV (prop.) at 3.34GHz which happens to be first resonance frequency. The analysis is performed by the excitation of only port 1 and port 2 is terminated and vice-versa as depicted in Fig. 4 and Fig. 5 respectively.

The performance of antennas from Ant. 0 to Ant. IV (prop.) can also be confirmed with respect to maximum and minimum isolation and percentage of efficiencies variations as shown in Figs. 6(a & b) respectively. Fig. 6(a) shows that Ant. 0 is associated with an isolation of 6.7dB. Further, Ant. I displays minimum isolation of 5.8dB which keeps on increasing till Ant. IV (prop.) for which the minimum isolation is 20dB. The maximum simulated isolation for Ant.0 is 20.18dB which keeps on increasing till Ant. II (54.69dB) while Ant. IV (prop.) displays maximum isolation of 33.5dB. Similarly, the minimum and maximum simulated efficiency (%) vary from 50 – 79 and 70 – 95.3 respectively. From

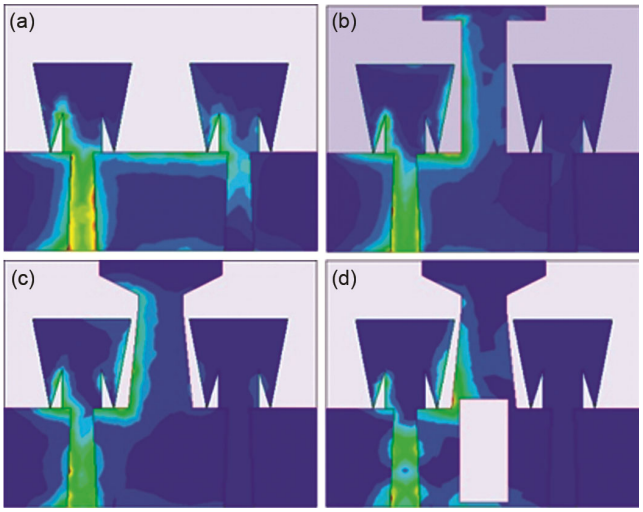

Fig. 4 — Current distributions at 3.34GHz by exciting port 1 and port 2 terminated for (a) Ant. I (b) Ant. II (c) Ant. III and (d) Ant. IV (prop.)

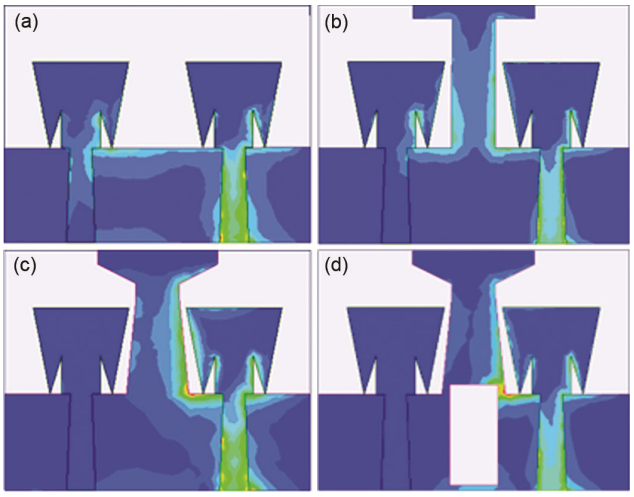

Fig. 5 — Current distributions at 3.34GHz by exciting port 2 and port 1 terminated for (a) Ant. I (b) Ant. II(c) Ant. III and (d) Ant.IV (prop.)

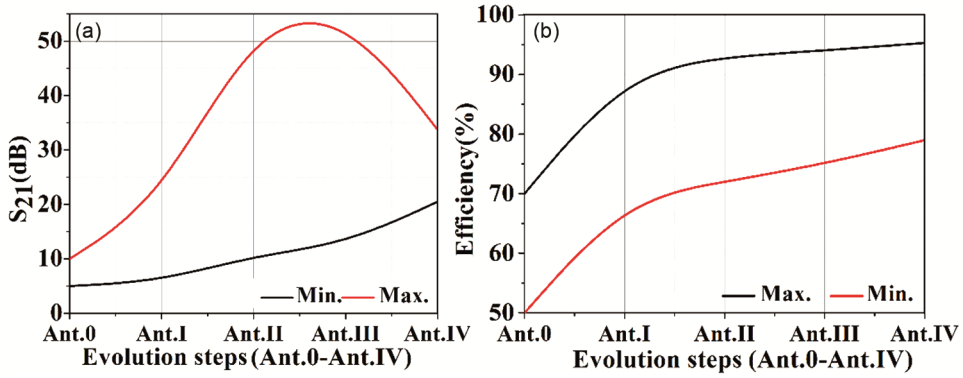

Fig. 6 — Maxima and minima enhancement of (a) $|S_{21}|$ and (b) Efficiency (%) for evolution steps

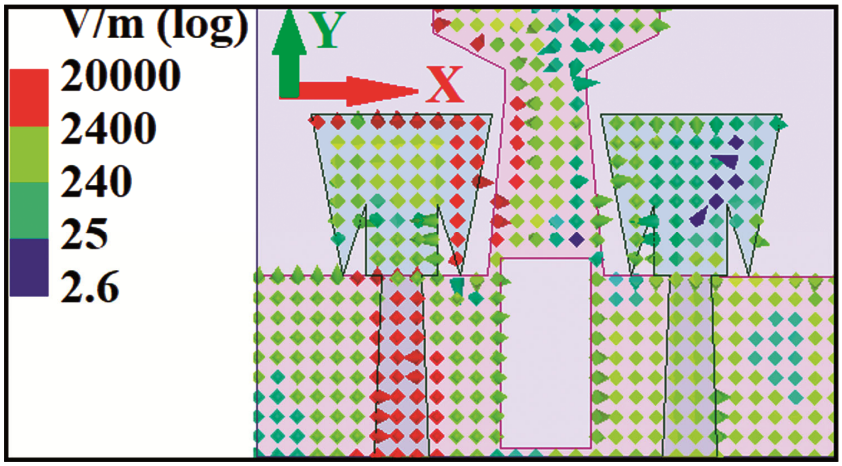

Fig. 7— E-Field distribution of the propose MIMO antenna at 3.34 GHz in *xy*- plane

Fig. 6(b), it is confirmed that the efficiency is gradually increased from Ant. 0 to Ant. IV (prop.) with stable maximum percentage of efficiency.

The proposed antenna E-field distribution is plotted in Fig. 7 to obtain the mode of operation at 3.34 GHz. From Fig. 7, it is evident that the electric fields (E-field) are distributed for the excited antenna 1 with half wavelength variation in the $+y$ direction (to edge), whereas the E-field is distributed in the opposite direction at the side edge of the patch. The demonstration of electric field distribution yielding the antenna 1 is operated in normal TM_{01} mode. A similar type of E-field distribution is obtained from antenna 2 for the mutual coupling. Hence, the coupling mode of antenna 2 is also excited with TM_{01} mode[42].

2.2.3 Parametric study

Short parametric studies have been carried out to confirm the proposed work. The S-parameter resulting from simulation of the MIMO antenna through different L_s and W_s values are shown in Fig. 8(a & b)

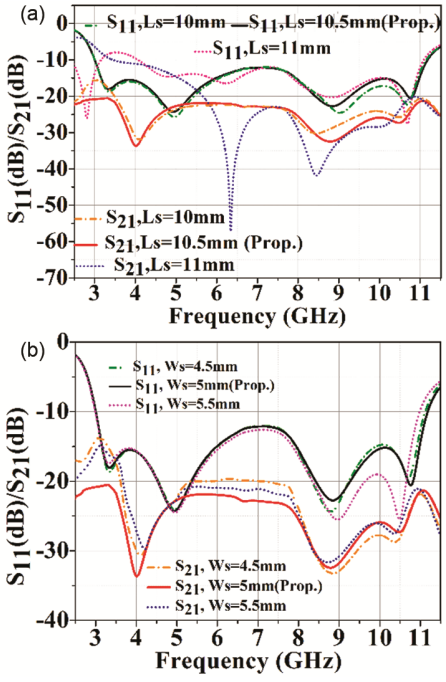

Fig. 8 — S_{11} and S_{21} responses for the variation of (a) parameter L_s and (b) parameter W_s

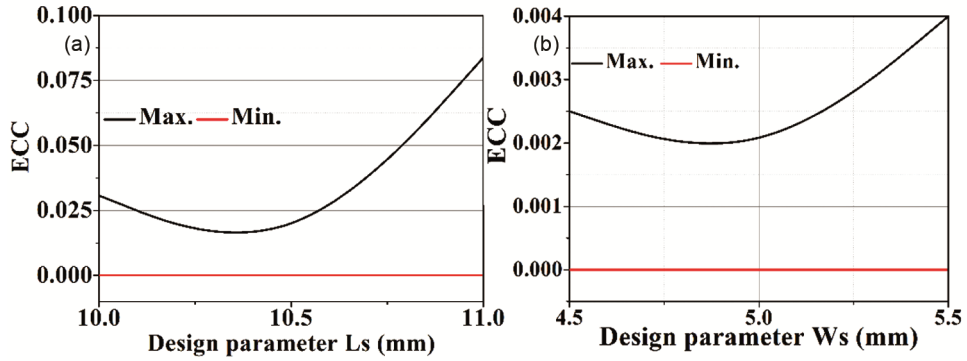

Fig. 9 — ECC variation for various values of (a) Parameter L_s and (b) Parameter W_s

respectively for comparison with other parameters being the dimensional values recorded in Table I.

From Fig. 8(a), it is clear that the highest isolation can be achieved when L_s = 10.5 mm (proposed) besides providing the widest impedance bandwidth (3.0 GHz - 11.22 GHz). When the L_s is increased by 0.5 mm (L_s = 11mm), the isolation at the lower frequency decreases (S_{21}< 15dB) up to 5 GHz while there is a shift of lower frequency to the right, thus narrowing the operating band (3.9 GHz to 11.2 GHz). This shows there is poor impedance matching in the lower frequency regions (3 GHz- 5 GHz). When L_s is decreased by 0.5mm ($L_s = 10\ mm$)from that of the proposed work, the impedance bandwidth is found to be from 3.02 GHz to 11.19 GHz while the isolation at the lower frequency is lower than 15dB due to the impedance matching problem at the lower frequency regions. Thus, optimum results are obtained when $L_s = 10.5\ mm$ as there is acceptable impedance matching at this point. Similarly, simulated S-parameters with different W_s values are presented in Fig. 8(b). The range of impedance bandwidth is 8.13 GHz (3.0 – 11.13 GHz), and isolation is lower than 15 dB at the lower frequency regions when $W_s = 4.5\ mm$ due to poor impedance matching at lower frequency regions (3.1 GHz - 3.6 GHz). At $W_s = 5.5\ mm$, impedance bandwidth lies between 3.0 GHz and 11.0 GHz, and the isolation is also found to be lower than 15 dB in the lower frequency regions. This shows there is an issue with impedance matching in this case. However, at $W_S = 5\ mm$ (proposed), there is more impedance matching as the impedance bandwidth is found to be 3-11.22 GHz and the isolation throughout the operating spectrum is greater than 20 dB. Thus, optimum results are confirmed when $W_S = 5\ mm$.

The parametric study can also be confirmed from the ECC variations for various values of parameter L_s and W_s shown in Fig. 9. The maximum ECC value of0.08 is obtained when $L_s = 11mm$ while it is 0.0015 when $L_s = 10.5mm$ (proposed) as shown in Fig. 9(a). Similarly, the maximum simulated ECC values for $W_s = 5.5mm$ and $W_s = 5mm$ (proposed) are 0.004 and 0.0015 respectively as shown in Fig. 8(b). The minimum simulated ECC values for all the cases are 0. Hence, it is confirmed that the proposed antenna has optimum performance in terms of ECC as well.

3 Results and Discussion

This section of the paper discusses and compares the various parameters with respect to simulated and measured results. The final hardware (fabricated) design of the proposed antenna was made to test inside an anechoic chamber to measure the parameters. The fabricated design acts as a receiver antenna which is placed at a distance of 3.25m from the transmitter as shown in Fig. 10 (a & b).

3.1 S-Parameter

The S-Parameter of the fabricated UWB MIMO antenna presented in Fig. 10(c) is measured by using ZNB 20 VNA (Vector Network Analyzer). Fig. 10(d) shows the simulated and measured S- parameters response.

The figure indicates that the impedance bandwidth ($S_{11} \leq -10$dB) obtained from measurement is 3.0-11.66 GHz with isolation (S_{21}) greater than 20dB throughout the working spectrum. This satisfies the bandwidth requirement for UWB applications. From the figure, it is noticed that S_{11} and S_{21} resulting from simulation and measurement have got some discrepancies which are mainly because of the effects of measurement environment and the cables used in the measurement.

3.2 Radiation characteristics

The co- and cross polarized radiation patterns (simulated and measured) of the proposed antenna under E and H-plane at resonant frequencies of 3.34,

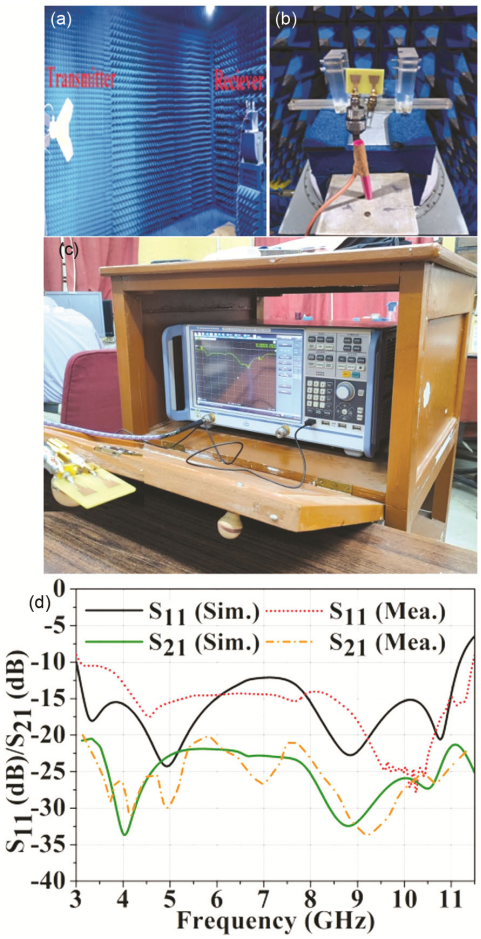

Fig. 10 — (a,b) Measurement set up in Anechoic chamber, (c) S-parameter measurement stage using VNA and (d) simulated and measured S-parameter

5.08 and 8.6GHz, are plotted in Figs. 11 & 12 when port_1 and port_2 are individually excited and other is terminated with a 50Ω load. The measurement of radiation patterns is done in an anechoic chamber as shown in Fig. 10.

Fig.11 and Fig.12 show that radiation patterns are pseudo-omnidirectional for both the ports being excited individually. The linearly polarized nature of the antenna is also confirmed as isolation of more than 20 dB is observed for the co- and cross polarized radiation patterns for the main lobe.

The co- and cross- polarization radiating power is constant throughout the angle θ, as shown in Fig. 13. Fig. 14(a) gives the gain value obtained from simulation and measurement. It is seen that both the simulated and measured values of gain have got very little amount of discrepancies. Further, the simulated peak gain varies from -0.0045dBi to 3.52dBi

3.3 Diversity characteristics

To examine diversity of any MIMO antenna, the required parameters are envelope correlation coefficient (ECC) and the diversity gain (DG). The use of ECC is to approximate correlation among the radiation patterns. So, ECC is employed to evaluate the isolation and relationship between the antenna elements. The ECC can be calculated by utilizing the far-field equation given in Eq. 3[39] respectively.

$$\rho_e = \frac{|\iint \vec{F_1}(\theta,\varphi).\vec{F_2}(\theta,\varphi)]d\Omega|^2}{\iint |\vec{F_1}(\theta,\varphi)|^2 d\Omega \iint |\vec{F_2}(\theta,\varphi)|^2 d\Omega} \quad \ldots (3)$$

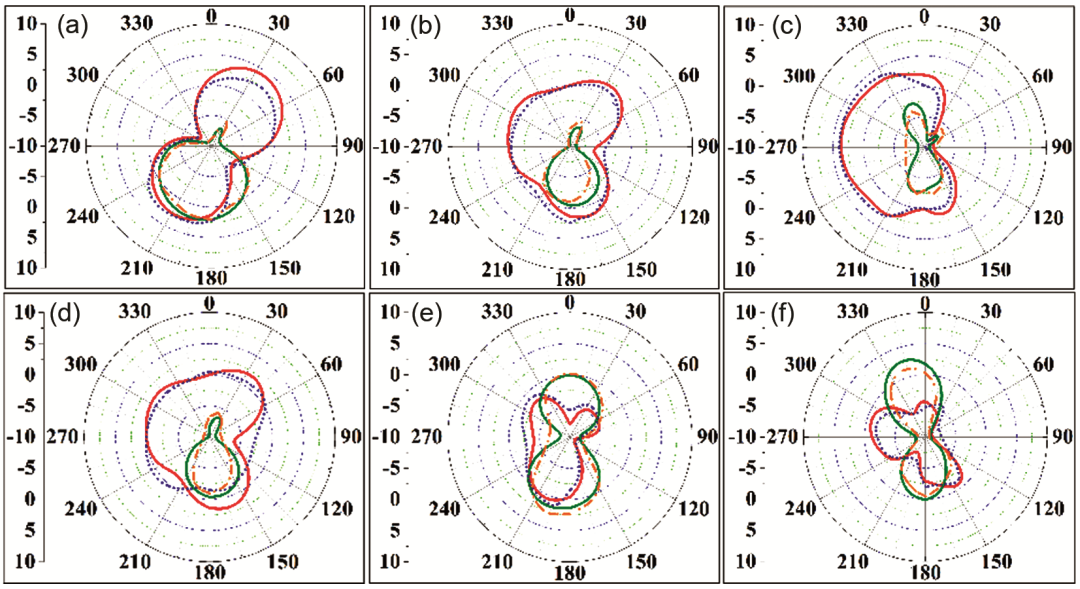

Fig. 11 — Co- and cross polarized far – field radiation patterns of the proposed MIMO antenna for only port-1 excitation under E – plane at (a) 3.34GHz, (b) 5.08GHz, (c) 8.6GHz and under H – plane at (d) 3.34GHz, (e) 5.08GHz, (f) 8.6GHz

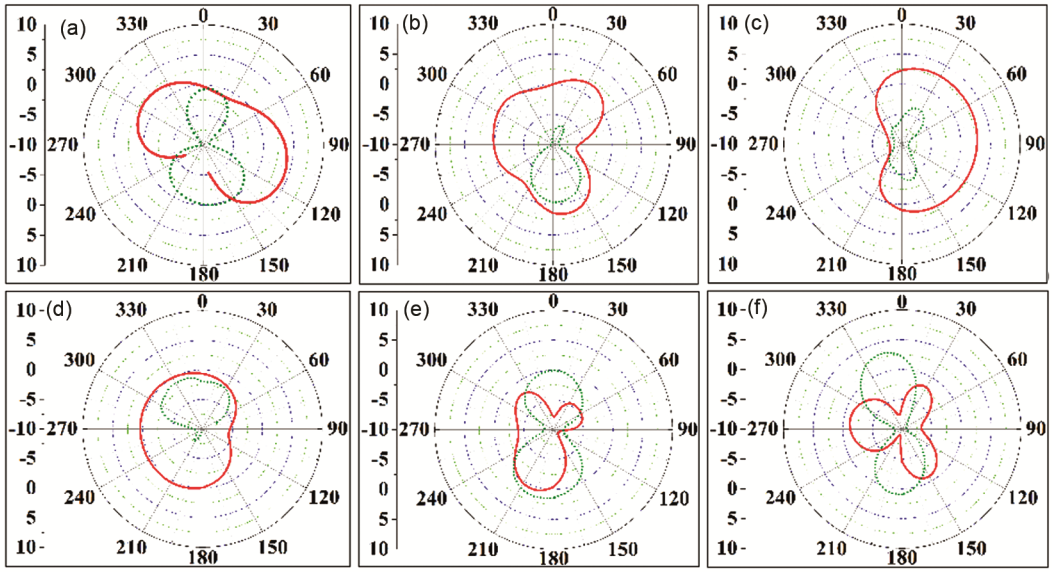

Fig. 12 — Co- and cross polarized far – field radiation patterns of the proposed MIMO antenna for only port-2 excitation under H– plane at (a) 3.34GHz, (b) 5.08GHz, (c) 8.6GHz and under H – plane at (d) 3.34GHz, (e) 5.08GHz, (f) 8.6GHz

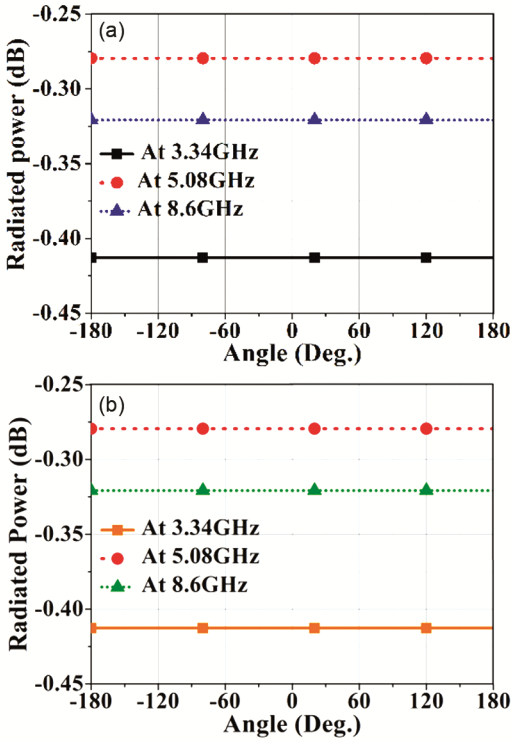

Fig. 13 — Simulated radiated power at 3.34, 5.08 and 8.6GHz for (a) Co-polarization and (b) Cross-polarization

where $\overrightarrow{F_1}(\theta,\varphi)$ and $\overrightarrow{F_2}(\theta,\varphi)$represents the radiated field patterns of Antenna 1 and Antenna 2 respectively, and ECC must be zero for an uncorrelated diversity antenna.

The ECC and diversity gain (DG) obtained from simulation and measurement are given in

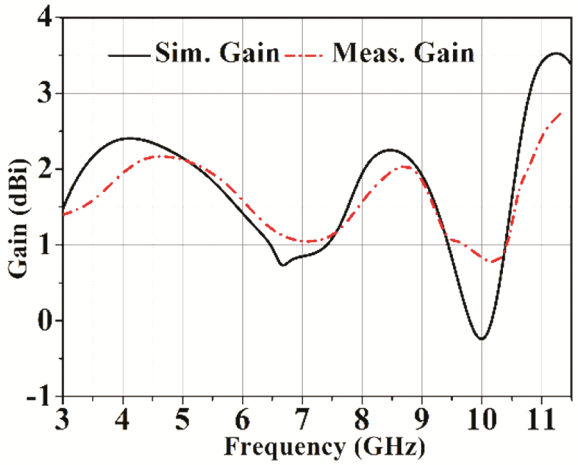

Fig. 14 — Simulated and measured Gain

Fig. 15 (a & b) respectively. The graphs signify that the ECC values resulting from simulation and measurement are lower than 0.01 throughout the working spectrum which is lower than the maximum permissible value of 0.5[39]. Moreover, the diversity gain (DG) is more than 9.98dBi throughout working spectrum. The DG can be calculated by using Eq.4[18].

$$DG = 10\sqrt{1-|\rho_e|^2} \quad \ldots (4)$$

The Channel Capacity Loss (CCL) obtained from simulation and measurement is found to be 0.25 bits/S/Hz which is less than 0.4 bits/S/Hz (maximum attainable)[35] throughout the working spectrum, as depicted in Fig. 16. It is calculated by using Eq. 5[40].

$$CCL = -log_2 \det(\alpha^R) \quad \ldots (5)$$

Where, $\alpha^R = \begin{bmatrix} \alpha_{11} & \alpha_{12} \\ \alpha_{21} & \alpha_{22} \end{bmatrix}$,

$$\alpha_{ii} = 1 - \left(\sum_{j=1}^{N} |S_{ij}|^2 \right), \alpha_{ij} = -(S_{ii}^* S_{ij} + S_{ji}^* S_{ij})$$

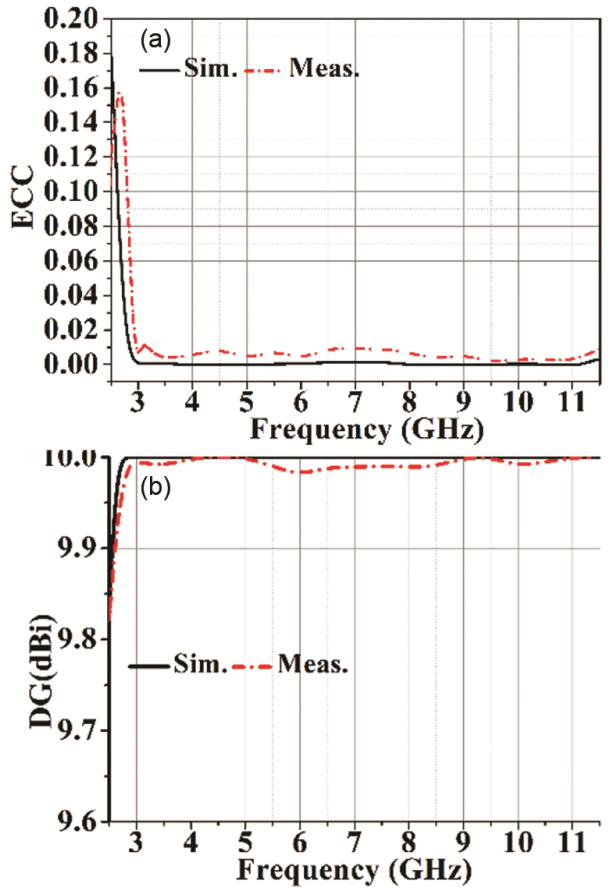

Fig. 15 — Simulated and measured response of (a) ECC and (b) DG

The proposed antenna performance comparisons with other previously available literatures are shown in Table 2.

3.4 Time Domain Analysis

The group delay and phase response (time domain) for the proposed MIMO antenna is shown in Fig. 17. The group delay analysis is performed by placing the antenna face to face and side by side configurations. The antennas are positioned in the far-field zone by maintaining a distance of 110mm with respect to each other in both the cases. From Fig. 17(a), it is seen that group delay lies between 1.43ns and -0.51ns throughout the working spectrum which is under tolerable limit[41] of MIMO antenna. The phase response for S_{11} parameter of the MIMO antenna has also been done. It is also observed from Fig. 17(b) that the phase varies linearly throughout the working spectrum.

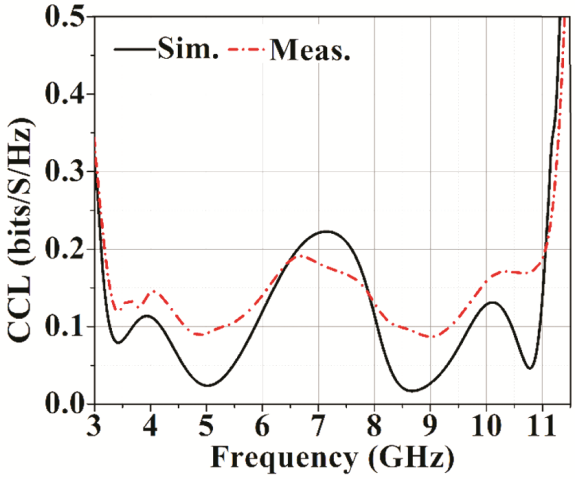

Fig. 16 — Simulated and measured CCL (bits/S/Hz)of the proposed MIMO antenna

Table 2 — Comparison of the proposed work with other works in the literature:$\lambda_0$is free space wavelength at lowest resonance. (PDM: Physical Dimension, EDM: Electrical Dimension BW: Bandwidth, PG: Peak gain, IS: Isolation)

Ref.	PDM (mm^2)	EDM $(\lambda_0)^2$	BW (GHz)	IS (dB)	PG (dBi)	ECC
[2]	29.5 × 60	0.41 × 0.82	3-20	> 23	-	0.001
[7]	36.6 × 39	0.76 × 0.44	3-10	> 30	4.9	-
[8]	90 × 100	0.5 × 0.4	2.43-12	> 15	4.51	-
[17]	50 × 80	0.32 × 0.45	3.3-20	> 20	6	0.06
[18]	50 × 35	0.25 × 0.30	2.9-12	> 15	6.5	0.004
[19]	35 × 35	0.52 × 0.36	3-11	> 25	-	0.3
[28]	30 × 30	0.62 × 0.62	5.8-15	> 25	6.2	0.07
[41]	45 × 25	0.58 × 0.33	3-12	> 15	5.4	0.2
Pro.	25 × 32	0.28 × 0.36	3-11.22	> 20	3.52	0.01

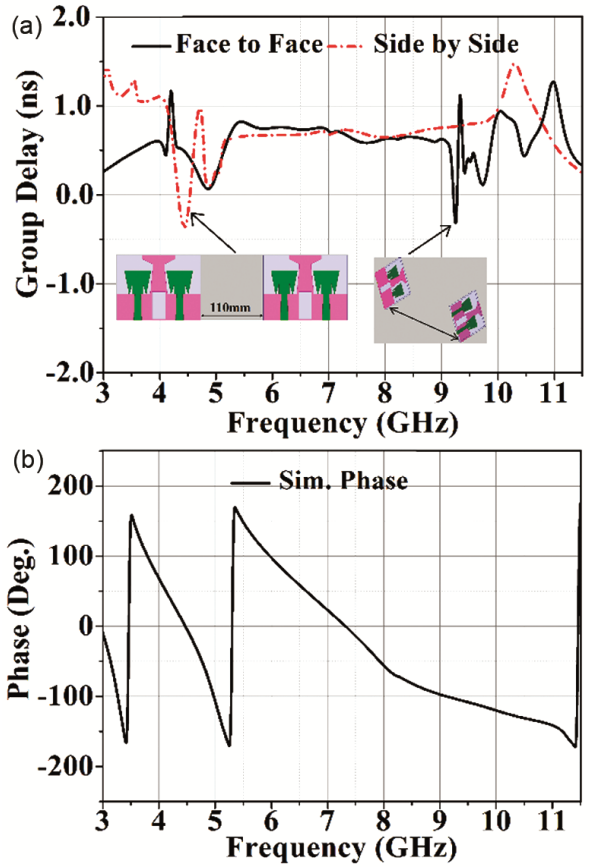

Fig. 17 — Time domain responses of the proposed MIMO antenna. (a) Group delay (ns) and (b) Phase response (Deg.)

The time domain analysis confirms that the distortion less transmission of signal as the responses is within the limit.

4 Conclusion

A compact two-port UWB symmetric MIMO antenna structure is developed on FR4 substrate. The antenna uses a modified T-shaped structure as a ground stub with a vertical slot to enhance the isolation and impedance bandwidth simultaneously. The measured impedance bandwidth of 3.0 - 11.66 GHz is covered with a minimum isolation of 20 dB throughout the working spectrum. Moreover, greater diversity in the MIMO operation has been confirmed. The respective ECC value and diversity gain of <0.01 and >9.98 dBi confirm the good signal quality of the MIMO system. The peak gain of 3.52 dBi is confirmed with a broad impedance bandwidth. The proposed MIMO can be superior in UWB applications in comparison to the work available in the open literature.

References

1 Jetti C R & Nandanavanam V R, *Int J Electron Commun,* 83 (2018) 11.
2 Bazil T A & Ivan F R, *Wireless Networks,* 28 (2022) 1977.
3 Zicheng N, Hou Z, Qiyang C & Tao Z, *IEEE Antennas Wireless Propag Lett,* 18 (2019) 1686.
4 Ricardo G V & Hildeverto J A, *IEEE Antennas Wireless Propag Lett,* 18 (2019) 2543.
5 Ameen M & Raghvendra K C, *IEEE Trnas Circuits Syst II: Expert Briefs,* 70 (2023) 1966.
6 Guo Z, Tian H, Wang X, et al., *IEEE Antennas Wireless Propag Lett,* 12 (2013) 1550.
7 Yeboah-Akowuah B, Kosmas P & Chen Y, *IEEE Trans Antennas Propag,* 65 (2017) 5069.
8 Xu R, Li J, Liu J, Zhou S G & Wei K, *Electron Lett,*54 (2018) 918.
9 Koziel S & Ul Haq M A, *IET Microwaves, Antennas Propag,* 12 (2018) 1360.
10 Garcia Z I J, Elmirghani J M H & Batchelor J C, *Novel Appl UWB Technol,* 10 (2011) 195.
11 Poonam T, Meenu K, Anshuman S, *et al*., *First Int Conf Microwave, Antenna Commun (MAC),*2023.
12 Poonam T, Meenu K, Anshuman S & et al., *Int J Electron Commun,* 184 (2024) 155411.
13 Vasu Babu K & Anuradha B, *Wireless Personal Commun,* 118 (2021) 3469.
14 Vandana S & Shikha N, *Wireless Personal Commun,* 98 (2018) 2901.
15 Roshna T K, Deepak U, Sajitha V R, Vasudevan K & Mohanan P, *IEEE Trans Antennas Propag,* 63 (2015) 1873.
16 Zhang S & Pedersen G F, *IEEE Antennas Wireless Propag Lett,* 15 (2016) 166.
17 Jehangir S S & Sharawi M S, *IEEE Antennas Wireless Propag Lett,* 16 (2017) 2320.
18 Wang L, Du Z, Yang H, Ma R, Zhao Y, Cui X & Xi X, *IEEE Antennas Wireless Propag Lett,*18 (2019) 1641.
19 Zhu J, Li S, Feng B, Deng L & Yin S, *IEEE Antennas Wirel Propag Lett,* 15 (2016) 905.
20 Tripathi S, Mohan A & Yadav S, *IEEE Antennas Wirel Propag Lett,* 14 (2015) 1565.
21 Zhang S, Lau B K, Sunesson A & He S, *IEEE Trans Antennas Propag,* 60 (2012) 4372.
22 Yang Z X, Yang H C, Hong J S & Li Y, *Microw Opt Technol Lett,* 58 (2016) 642.
23 Fella G & Mouloud C, *Wireless Personal Commun,* 128 (2023) 131.
24 Li W, Hei Y, Grubb PM, Shi X & Chen R T, *IEEE Access*, 6 (2018) 50290.
25 Suriya I & Anbazhagan R, *Int J Electron Commun,* 99 (2019) 25.
26 Liu L, Cheung S & Yuk T, *IEEE Trans Antennas Propag,* 63 (2015) 1917.
27 Niraj K & Usha K, *Wireless Personal Commun,* 127 (2020) 153423.
28 Mekala H R, Sheela D, Vinay K P & Abhay S, *Microsystem Technol*, 27 (2021) 1971.
29 Ashutosh M & Bikash R B, *Int J Electron Commun,* 124 (2020) 153361.
30 Muzammil S M, Rakesh C & Raghvendra K C, *IEEE Access,* 8 (2020) 139658.

31 Jayant K R, Anuragi K, Naveen M, et al., *Int J Electron Commun,* 176 (2024) 155120.

32 Jayant K R, Pinku R & Rakesh C, *Int J Electron Commun,* 171 (2023) 154872.

33 Jayant K R, Pratika K, Abhishek S, et al., *3rd Asian Conference on Innovation in Technology (ASIANCON)*, 2023.

34 Weng Y F, Cheung S W & Yuk T I, *Microwave Opt Technol Lett,* 53 (2011) *523.*

35 Liu L, Cheung S W & Yuk T I, *PIERS Proc,* (2011) 1420.

36 Liu L, Cheung S W, Azim R & Islam M T, *Microwave Opt Technol Lett,* 53 (2011) 2283.

37 Deepak K B, Kalyan M &Azharuddin M, *Microwave Opt Technol Lett,* 65 (2023) *2384.*

38 Bazil T A & Ivan F R, *Wireless Networks,* 18 (2022) 1977.

39 Alsath M G N & Kanagasabai M, *IEEE Trans Antennas Propag,* 63 (2015) 4204.

40 Kumar A, Ansari A Q, Kanaujia B K, Kishor J & Kumar S, *Int J Electron Commun,* 114 (2020) 152997.

41 Mathur R & Dwari S, *Int J Electron Commun*, 93 (2018) 1.

42 Li M, Zhong B G & Cheung S W, *IEEE Trans Antennas Propag,* 67 (2019) 755.